This version is available at https://strathprints.strath.ac.uk/62467/

Power Dispatch and Voltage Control in Multi-terminal HVDC Systems: A Flexible Approach

Ali Raza, Liu Yuchao, Kumars Rouzbehi, *Senior Member*, *IEEE,* Mohsin Jamil, Syed Omer Gilani, Xu Dianguo, *Fellow*, *IEEE*, Barry W. Williams

Abstract—This paper deals with the power dispatch and direct voltage control in multi-terminal high voltage direct current (MT-HVDC) systems. Generalized voltage droop (GVD) control is adopted for Voltage Source Converters (VSC)s of a MT-HVDC system. A mechanism has been designed based on the power ratio within the GVD controlled stations to achieve flexible autonomous coordination control among VSC-HVDC stations, without need for communication. In this study, several alternatives are considered to guarantee fault ride through of onshore converter stations. The performance of the proposed control strategy is analyzed with time-domain dynamic simulations, in an EMDTC/PSCAD platform, and experimentally validated. Results demonstrate the robust performance and capabilities of the proposed control strategy during changes in the power demand of the ac grids, unexpected change in wind power generation, and eventual permanent VSC-HVDC station disconnection.

Index Terms— dc voltage droop control, offshore wind farms, power dispatch, VSC based multi-terminal HVDC grids.

I. INTRODUCTION

WITH advances in power electronics technology, multi-terminal high voltage direct current (MT-HVDC) systems/grids have become a technically and economically feasible solution for grid integration of renewable energy resources [1].

Several MT-HVDC systems have been installed, successful

A. Raza is with the Department of Robotic and AI, National University of Sciences and Technology, Pakistan (e-mail: i.will.rize@gmail.com).

L. Yuchao and X. Dianguo are with the School of Electrical Engineering and Automation, Harbin Institute of Technology, Harbin 150001, China (e-mail:liuyuchaohit@outlook.com; xudiang@hit.edu.cn;).

K. Rouzbehi is with the Electrical Engineering Department, Technical University of Catalonia, Spain. (e-mail: q.rouzbehi@gmail.com)

M. Jamil and S. O. Gilani are with the Department of Robotic and AI, National University of Sciences and Technology, Pakistan (e-mail: mohsin@smme.nust.edu.pk; omer@smme.nust.edu.pk).

B. W. Williams is with the University of Strathclyde, Glasgow G1 1XW, U.K. (e-mail: Barry.Williams@strath.ac.uk).

examples are the Nanao project (commissioned on 2013), and the Zhoushan project (commissioned on 2014) in China. Moreover, there are several promising proposals/under construction such as; an MT-HVDC system for interconnecting the Nordik pool with continental Europe, and the 4-terminal HVDC system of Zhangbei (to be commissioned in 2018).

Voltage source converter (VSC) HVDC technology is becoming the building block for the integration of wind farms (WFs) in HVDC systems. VSC-HVDC technology is a superior solution to its traditional counterpart (Line Commutated Converter (LCC)-HVDC systems) because of its independent controllability of active and reactive power, ability to supply passive ac networks, capability to change the power flow direction without need to change the power converter polarity.

An MT-HVDC system/grid is typically formed by a number of grid side VSC (GS-VSC) and wind farm side VSC (WF-VSC) stations located at different geographical positions. Development of MT-HVDC grids brings several technical challenges that should be addressed. The main challenges are system operation, dc voltage control, power dispatch, and protection [2].

Several studies have been conducted into dc voltage control and power sharing of MT-HVDC grids. The main control strategies can be classified as master-slave, voltage margin and voltage droop. In master slave control, the slack converter controls the dc voltages and the other converters operate in a power control mode. This method allows proper reference tracking, while the incorporation of frequency loops allows ac grid support [3]. However, dc voltage will be lost once the power of the slack converter reaches its rating or in the case of a slack converter outage. Voltage margin control overcomes these limitations by selectively changing the slack converter, once the dc voltage is not within the specified limit. The transient voltage oscillations resulting from changing the slack converter, are the main drawback of this strategy [4]. It is also shown in [4] that during a converter outage, voltage margin control operates satisfactory only when the tripped converter operates in a constant power control mode. Voltage droop control of MT-HVDC grids has been presented as a more reliable option for dc buses voltage control. The reason is that

droop control allows a number of converters to simultaneously participate in dc voltage regulation [5]–[9], which is similar to ac frequency regulation by a number of generators. However, the difference between droop control implemented based on local dc voltage measurements at each station and ac frequency control, is the lack of a common signal in the dc grid and much faster dynamics associated with dc voltage control [10]. This in turn results in poor reference tracking in the MT-HVDC system. Moreover, load sharing is not explicitly dependent on the droop parameters but is also determined by the line parameters, which makes it difficult to plan exact power sharing.

A control method consisting of both voltage margin and droop control for reliable operation of MT-HVDC connecting oil platforms and offshore WFs, is presented in [11]. Lie Xu *et al.* have presented an interesting method of coordinated droop control for power sharing within MT-HVDC grid [12]. Three management schemes with control principles are proposed in [13]. Generally, analysis of the dc-link voltage is missing which is critical from a design perspective.

This paper advances direct voltage control and power dispatch flexibility, and enhances the capability of MT-HVDC transmission systems for integration of offshore wind farms during both steady-state and ac fault conditions. The proposed philosophy highlights and validates the power dispatch flexibility for MT-HVDC grids as a step towards the realization of MT-HVDC grids. A detailed study into two proposed control schemes for power dispatch based on transmission ratio with GVD during steady state and abnormal operations, including the selection of control parameters based on a VSC station's dc voltage variation, is validated by simulation and experimentation. Investigation into various techniques for ensuring fault ride through (FRT) of the mainland grid fault is also carried out. The proposed FRT strategy, based on GVD, for active power sharing is validated through simulation and experimentation.

This paper is structured as follows: section II presents the layout of the four-terminal VSC-HVDC test system and power flow analysis. Flexible power dispatch and dc voltage control strategies are presented in section III. The GVD coefficients are calculated based on the power sharing ratio to ensure the system FRT capability and dc voltage control during onshore ac grid faults. In Section IV, different FRT strategies are discussed and a strategy is presented based on GVD and overvoltage control. The proposed control strategy is investigated and assessed via EMTDC/PSCAD simulations and validated by scale-down laboratory experimentation, in section V. Finally, remarks and conclusions are drawn.

II. System Description and Power Flow Equation

In order to analyze the proposed control structure, a four-terminal VSC-HVDC transmission system of two onshore ac grids and two offshore WFs is considered as shown in Fig. 1. In the system, R_1 to R_5 are cable dc resistances, I_{dc1} to I_{dc4}, and V_{dc1} to V_{dc4} are the dc currents and voltages of the VSCs [14]. I_{dc5} is the summation of I_{dc1} and I_{dc2} through R_5. The relationships between the dc currents and voltages are:

$$V_{dc1} = V_x + I_{dc1}\,R_1 \tag{1}$$

$$V_{dc2} = V_x + I_{dc2}\,R_2 \tag{2}$$

$$V_{dc3} = V_y - I_{dc3}\,R_3 \tag{3}$$

$$V_{dc4} = V_y - I_{dc4}\,R_4 \tag{4}$$

$$V_x = V_y + I_{dc5}\,R_5 \tag{5}$$

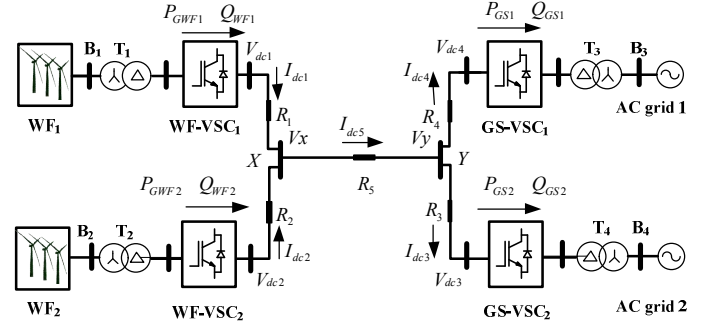$$I_{dc5} = I_{dc1} + I_{dc2} = I_{dc3} + I_{dc4} \tag{6}$$

Fig. 1. Four-terminal VSC system under study.

By taking I_{dc1}, I_{dc3}, I_{dc4} and V_{dc2} as inputs, (1) to (6) can be expressed as:

$$V_{dc1} = (R_1 + R_2)I_{dc1} - R_2\,I_{dc3} - R_2\,I_{dc4} + V_{dc2} \tag{7}$$

$$V_{dc3} = R_2\,I_{dc1} - (R_2 + R_3 + R_5)I_{dc3} \\ - (R_2 + R_5)I_{dc4} + V_{dc2} \tag{8}$$

$$V_{dc4} = R_2\,I_{dc1} - (R_2 + R_3)I_{dc3} \\ - (R_2 + R_4 + R_5)I_{dc4} + V_{dc2} \tag{9}$$

$$I_{dc2} = I_{dc3} + I_{dc4} - I_{dc1} \tag{10}$$

The MT-HVDC system equations become:

$$\begin{bmatrix} V_{dc1} \\ V_{dc3} \\ V_{dc4} \\ I_{dc2} \end{bmatrix} = \begin{bmatrix} R_1 + R_2 & -R_2 & -R_2 & 1 \\ R_2 & -(R_2 + R_3 + R_5) & -(R_2 + R_5) & 1 \\ R_2 & -(R_2 + R_2) & -(R_2 + R_4 + R_5) & 1 \\ -1 & 1 & 1 & 0 \end{bmatrix} \begin{bmatrix} I_{dc1} \\ I_{dc2} \\ I_{dc3} \\ I_{dc2} \end{bmatrix} \tag{11}$$

Power flow of the VSC-HVDC stations are:

$$P_{WF1} = V_{dc1}\,I_{dc1} \qquad\qquad P_{WF2} = V_{dc2}\,I_{dc2}$$

$$P_{GS1} = V_{dc3}\,I_{dc3} \qquad\qquad P_{GS2} = V_{dc4}\,I_{dc4}$$

III. Flexible DC Voltage Control and Power Dispatch

Control of each VSC-HVDC station is done via two cascaded levels. Current control in the inner control layer is attained through vector control [15], and the outer control loop is implemented via decentralization that is designed to transmit generated power from WF-VSC to GS-VSC keeping the direct grid voltage in a safe operating range of ±5% [16], [17].

DC voltage control of the proposed control structure is realized by implementation of the GVD [18], based on a dual hierarchical structure and its operational modes are presented in Fig. 2. The GVD is expressed mathematically by:

$$\alpha V_{dc} + \beta P + \gamma = 0 \tag{12}$$

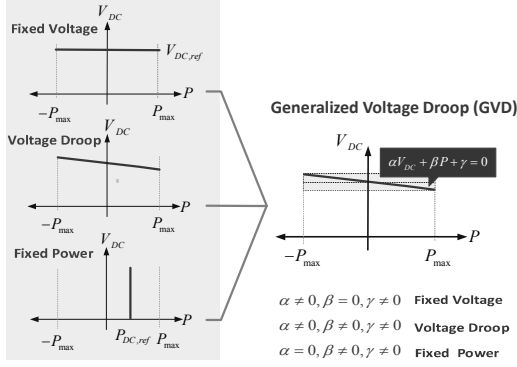

Fig. 2.GVD characteristics for deployed modes.

The coefficients α, β and γ mainly depend on the MT-HVDC system voltage and power [16], [18]. If a droop control mode is utilized, all the parameters will be non-zero. In this paper in order to the find parameters (α, β and γ) in (12), the GVD slope is assumed constant. Hence:

$$k = \frac{\beta}{\alpha}$$

Without loss of generality, assuming $\alpha = 1$ for conventional voltage droop control, yields:

$$\beta = k$$

Thus, γ is determined from (12) as:

$$\gamma = -V_{dco} - k\,P_o \tag{13}$$

where k is the voltage droop slope of the VSC station. In practice, a transmission system operator (TSO) may need to allocate the generated offshore wind energy in various ways under different circumstances. Thus, the objective of this sub-section is to signify the flexibility of MT-HVDC systems by adopting feasible operation for power dispatch from numerous plausible modes.
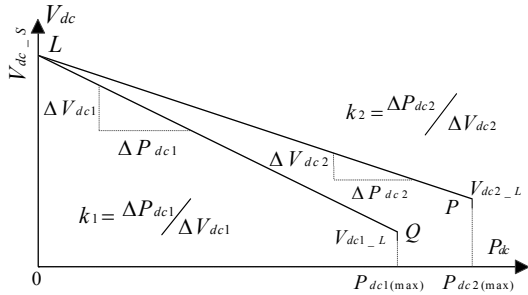

Fig. 3. Droop characteristics of VSCs for WF-VSCs.

1) *Droop controlled WF-VSCs:* Faults on any mainland ac grid forces the GS-VSCs to transfer into the current limitation mode. In this situation, WF-VSCs take responsibility for dc-link voltage regulation via GVD control.

In this study, GVD droop control on the WF-VSCs is considered when the generated wind power is transferred to the mainland grids based on the power transmission ratio $m = P_{WF1}/P_{WF2} = i_{dc1}/i_{dc2}$, that is, regulation and governance by the TSO. Fig. 3 illustrates the droop characteristics for two WF-VSCs along lines LQ and LP, and are:

$$I_{dc1} = k_1\,\Delta V_{dc1} = k_1(V_{dc\_s} - V_{dc1\_L}) \tag{14}$$

$$I_{dc2} = k_2\,\Delta V_{dc2} = k_2(V_{dc\_s} - V_{dc2\_L}) \tag{15}$$

Substituting (14) and (15) into (1) and (2), respectively, yields:

$$\frac{I_{dc1}}{I_{dc2}} = \frac{R_2 + \frac{1}{k_2}}{R_1 + \frac{1}{k_1}} = m \tag{16}$$

Thus, to keep the transmission ratio as m, droop characteristics need to be set as [14]:

$$k_2 = \frac{1}{m\,R_1 - R_2 + \left(\frac{m}{k_1}\right)} \tag{17}$$

Equation (17) shows the power transmission ratio only depends on the transmission line resistances seen from the common connection point to the respective VSC station, point X in this case shown in Fig. 1. The equivalent resistances perceived from the voltage droop characteristics, $1/k_1$ and $1/k_2$, are much higher than the actual line resistances R_1 and R_2. Therefore, (17) can be simplified to $k_2 = k_1/m = \beta_1/m = \beta_2$. Direct voltages at all VSCs are, taking into account Fig. 3 and equations (11) and (16):

$$\begin{bmatrix} V_{dc1} \\ V_{dc2} \\ V_{dc3} \\ V_{dc4} \end{bmatrix} = \begin{bmatrix} \frac{m}{k_1(m+1)} & \frac{m}{k_1(m+1)} & 1 \\ \frac{m}{k_2(m+1)} & \frac{m}{k_2(m+1)} & 1 \\ -R_3 - R_{25}' & -R_{25}' & 1 \\ -R_3 - \frac{R_2'}{m+1} & -R_4 - R_5 - \frac{R_2'}{m+1} & 1 \end{bmatrix} \begin{bmatrix} I_{dc3} \\ I_{dc4} \\ V_{dc\_S} \end{bmatrix} \tag{18}$$

where $R_{25}' = R_5 + \left[\frac{1}{m+1}(R_2 - \frac{1}{k_2})\right]$ and $R_2' = R_2 - \frac{1}{k_2}$.

The GVD coefficient γ for the WF-VSCs are:

$$\gamma_1 = -V_{dco} - k_1\,P_o \tag{19}$$

$$\gamma_2 = -V_{dco} - k_2\,P_o \tag{20}$$

GS-VSCs transfer the received power to the respective connected ac networks. Fixed ac voltage and active power control is applied to GS-VSC$_1$ while reactive and active power control is selected for GS-VSC$_2$.

2) *Droop controlled GS-VSCs:* GVD based droop control is employed for power coordination and dc voltage control on the GS-VSCs. Two GS-VSCs have a certain power ratio set by the utility, given by $m = P_{GS1}/P_{GS2} = i_{dc3}/i_{dc4}$. The lines LN and LM in Fig. 4 illustrate the dc droop characteristics for the GS-VSCs and are:

$$I_{dc3} = k_3\,\Delta V_{dc3} = k_3(V_{dc\_s} - V_{dc3\_h}) \tag{21}$$

$$I_{dc4} = k_4\,\Delta V_{dc4} = k_4(V_{dc\_s} - V_{dc4\_h}) \tag{22}$$

Substituting (21) and (22) into (3) and (4), respectively, produces:

$$\frac{I_{dc3}}{I_{dc4}} = \frac{R_4 + 1/k_4}{R_3 + 1/k_3} = m \tag{23}$$

and to preserve m, the droops of GS-VSCs are set to:

$$k_4 = \frac{1}{m R_3 - R_4 + \left(m/k_3\right)} \tag{24}$$

(24) can be simplified to $k_4 = k_3/m = \beta_3/m = \beta_4$ and the dc voltages at all four terminals are expressed in (25).
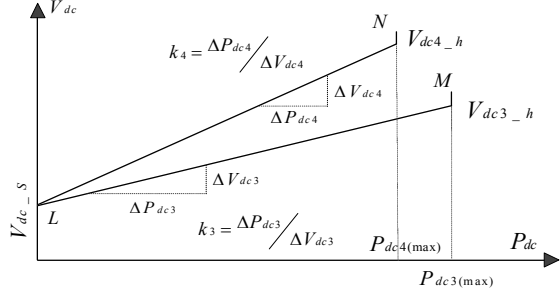

Fig. 4. Droop characteristics of VSCs for droop control on GS-VSCs.

$$\begin{bmatrix} V_{dc1} \\ V_{dc2} \\ V_{dc3} \\ V_{dc4} \end{bmatrix} = \begin{bmatrix} R_1 + R'_{35} & R'_{35} & 1 \\ R_2 + R'_{35} & R'_{35} & 1 \\ \dfrac{m}{k_3(m+1)} & \dfrac{m}{k_3(m+1)} & 1 \\ \dfrac{1}{k_4(m+1)} & \dfrac{1}{k_4(m+1)} & 1 \end{bmatrix} \begin{bmatrix} I_{dc1} \\ I_{dc2} \\ V_{dc\_S} \end{bmatrix} \tag{25}$$

where $R'_{35} = R_5 + R'_3 \, m/{m+1}$ and $R'_3 = R_3 - 1/k_3$.

The third GVD coefficient is calculated based on (13):

$$\gamma_3 = -V_{dco} - k_3 P_o \tag{26}$$

$$\gamma_4 = -V_{dco} - k_4 P_o \tag{27}$$

The purpose of the employed WF-VSC control is to preserve the ac voltage of WFs at a specific level. Voltages are produced at a constant 50 Hz frequency and the magnitude is controlled by proportional integral (PI) control, which improves accuracy and thus is used as a performance index for the controller [16].

IV. FAULT RIDE THROUGH OF MT-HVDC DURING ONSHORE AC GRID FAULT

An onshore ac grid fault or disconnection of its converter station affects the ac voltage at one or more GS-VSCs, depending on the ac network connections. To ensure fault ride through capability of the MT-HVDC system during such an occurrence, two conditions must be satisfied, as proposed by Lie Xu *et al.* in [14]:

1. AC voltage and frequency variations at offshore substations need to be maintained within a limited range, so that after mainland fault clearance, the system quickly returns to normal operation.

2. Active power generation must be balanced with power exchange under abnormal conditions. Energy exchange may significantly reduce between the relevant GS-VSC and ac grid during an ac fault. Since the ac voltage level drops, the total

power in MT-HVDC grid exceeds the generated WF power. This results in dc link overvoltage, leading to shut down of the whole MT-HVDC grid. In this scenario, the option is to reduce the extracted power to the system or supply extra available energy to other healthy ac networks, so as to maintain the dc-link voltage in a stable region.

The dc-link voltage is maintained by the GS-VSCs during normal operation but under abnormal conditions the voltage limits may be exceeded, due to reduced active power exchange between the GS-VSCs and the ac networks. Various techniques have been employed for active power balancing:

• *Strategy 1:* Frequency modulation of offshore ac networks. The frequency of the offshore ac grid is increased using a WF-VSC under a mainland grid fault, and power generation from wind turbines automatically reduce upon detection of an abnormal frequency [19]. Reliability and special wind turbine designs are the main concerns associated with this method.

• *Strategy 2:* DC damping resistors are switched in during dc link overvoltage, placed on the dc side of each GS-VSC [20], [21]. The damping resistors must be able to absorb the total generated power on each GS-VSC substation; adding a capital and operational cost.

• *Strategy 3:* Fast telecommunication between WF-VSCs and respective wind turbines. Upon detection of a dc-link overvoltage, a signal to all turbines allows the quick reduction of power generation [22]. This technique is difficult to implement in practice as even a short delay in communication can cause an unacceptable dc-link overvoltage [14].
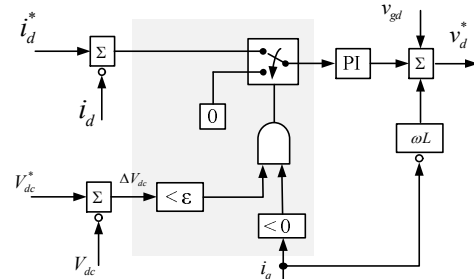

Fig. 5. Overvoltage control strategy.

In this study, an active power sharing strategy based on GVD is used to deal with the mentioned shortcomings. Excess power of the MT-HVDC system, upon detection of the dc-link overvoltage, is transferred to the healthy connected GS-VSC station. A dc overvoltage protection scheme with a permitted $\pm 5\%$ of the nominal dc-link voltage variation is implemented on each GS-VSC. In the proposed control strategy, no extra hardware, special wind turbine design or telecommunication is needed.

The principle of this approach is to transfer the excessive energy to an unaffected ac network during an onshore ac fault or disconnection. When the GS-VSC is connected or its connection lost instantaneously, a dc voltage spike results momentarily. The voltage spikes are associated with over-charging of the dc capacitors. Each GS-VSC is equipped with dc overvoltage protection as shown in Fig. 5 to satisfy the FRT conditions defined in [14]. Ratings of the VSC stations

are maintained slightly more than their base powers for soft power exchange and to avoid overloading. A VSC station will be temporarily disabled when ΔV_{dc} exceeds the limit (that is ε). Thus, the dc-link capacitor voltage drops because of discharging by an uninterrupted I_{dc} and the VSC station returns to normal operation. As discharge occurs quickly, the overvoltage scheme interacts for a short sub-second period [11].

V. SIMULATIONS AND EXPERIMENTAL RESULTS

EMTDC/PSCAD simulations and scaled-down laboratory experimental results of the proposed control strategy, under different test scenarios, establish the effectiveness of the proposed control structure. These tests are wind power change, sudden demand change from an onshore ac grid, and permanent disconnection of a GS-VSC due to a symmetrical ac grid fault. The last test is performed to verify the fault ride through capability of the MT-HVDC system and to confirm that the dc grid fulfills the FRT standards in [14].

The experimental set-up (Fig. 1) is shown in Fig. 6 while the parameters for the 4-terminal system and PI controllers are given in Table I and II, respectively. The nominal dc-link voltage is maintained at 1pu. Electrical characteristics of dc cables are given in Table III. The base values for dc-link voltage and power for normalization are 400V and 800W, respectively.

Fig. 6. Experimental platform of the test grid presented in Fig. 1.

Table I.
Parameters of the system

| System Parameters	Values
VSC stations topology	2-level
Grid voltage	400 V
Power rating of VSC stations	800 W
VSC stations coupling inductance	1.58 mH
Switching frequency	10.0 kHz

Table II.
PI and droop control parameters

PI Parameters	K_p	T_i
Wind farm ac voltage controller	1.00	1.0000
Active power controller	0.01	0.0400
Reactive power controller	0.00	0.3030
d-axis current controller	0.48	0.0067
q-axis current controller	0.48	0.0067

The active power references for WF-VSC$_1$, WF-VSC$_2$, GS-VSC$_1$ and GS-VSC$_2$ are 0.7pu, 0.3pu, -0.7pu and -0.3pu, respectively, while the power rating of each VSC is 800W.

The wind farm side VSCs are controlled to mimic infinite voltage sources to obtain a constant ac voltage and frequency, and to harvest maximum generated wind power [19], [22]. Control of the GS-VSCs is presented in section III.

Table III.
Equivalent parameters of each π sections of all the cables

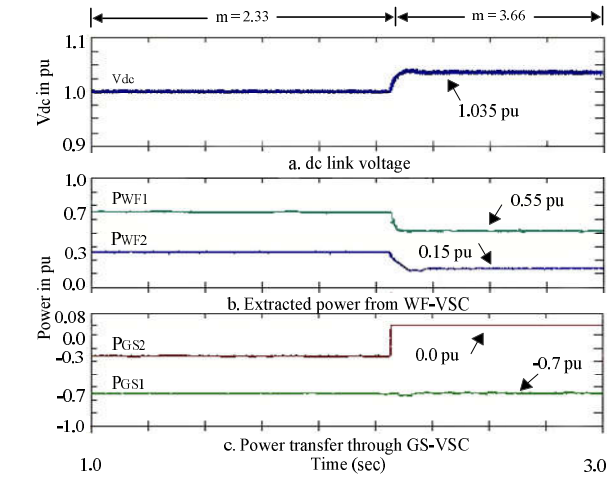| Parameters	Cable 1, 3	Cable 2, 4	Cable 5
dc resistance, mΩ	3.0	2.9	3.2
dc inductance, mH	2.8	1.4	2.8
dc capacitance, μF	1.0	0.7	1.0
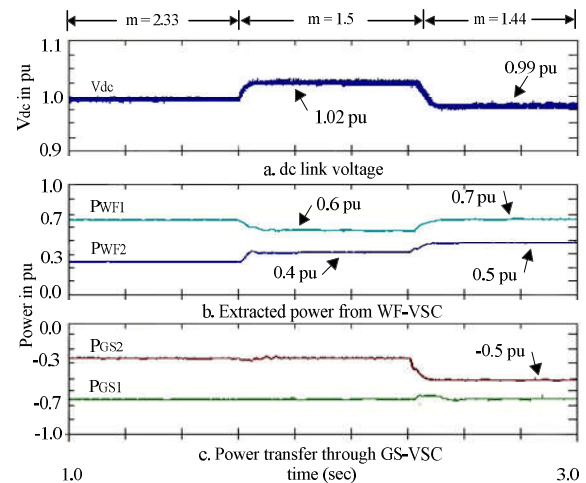
a. Simulation results
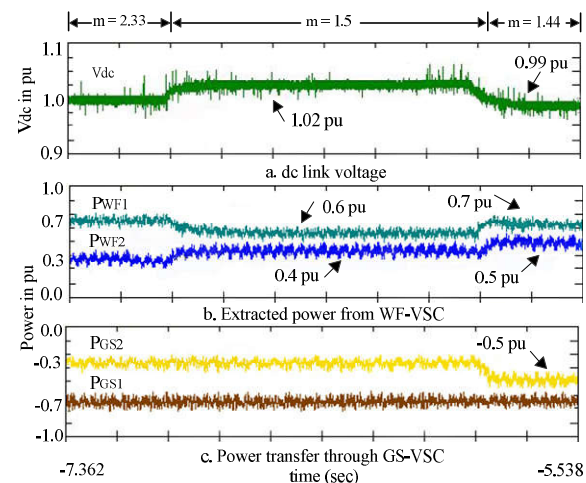
b. Experimental results

Fig. 7. DC-link voltage and power during change in power from WF-VSC$_1$ and GS-VSC$_1$ (test 1 and 2 - scheme 1).

1) Scheme 1: Simultaneous voltage sag appears on the onshore ac grids, so dc-link voltage control shifts to the WF-VSCs by GVD action. Initially, V_{dc-s} and V_{dc1-L} are set at 1.05pu and 0.95pu, respectively, which corresponds to the maximum dc current variation of 1pu (800W). Thus, the GVD characteristics k_1 for WF-VSC$_1$ is 10, using $k_1 = \Delta P_{dc}/\Delta V_{dc} = \Delta P_{dc}/V_{dc\_s} - V_{dc1\_L}$. Then, by using a simplified form of (17), $k_2 = k_1/m$. The value of k_2 is calculated as 4.29, 6.66, 7.14 and 2.73 for transmission ratios m of 2.33, 1.5 1.44 and 3.66, respectively.
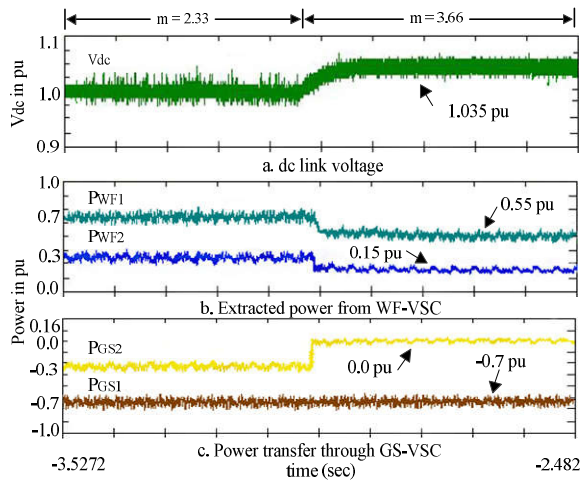
Operation during tests 1 and 2 is shown in Fig. 7. When the wind power of WF_2 is changed to 0.4pu, P_{WF1} reduces to 0.6pu and the dc voltage level shifts to 1.02pu, while power transfer through GS-VSCs remains constant with $m = 1.5$. In the second half of Fig. 7, a load demand change from GS-VSC$_1$ is assessed. P_{GS2} shifts to -0.5pu, P_{GS1} remains constant but power extraction from WF-VSC$_1$ and WF-VSC$_2$ increases as per the transmission ratio ($m = 1.44$), to 0.7pu and 0.5pu, respectively, to stabilize V_{dc} within ±5%, at 0.99pu.

a. Simulation results

b.   Experimental results

Fig. 8. DC-link voltage and power during disconnection of GS-VSC$_1$ to check FRT capability of system (test 3 – scheme 1).

To validate FRT capability of the grid side converter, permanent disconnection of GS-VSC$_2$ is observed due to a persistent symmetrical fault on the secondary side of the GS-VSC$_2$'s coupling transformer. The transmission ratio and overvoltage controller factor ε are 3.66 and 0.0015V, respectively. For such a scenario, the overvoltage controller stabilizes the system voltage to 1.035pu, while the power from WF$_1$ and WF$_2$ reduce to 0.55pu and 0.15pu, respectively, to ensure grid stability. Voltage and power profiles for the EMDTC/PSCAD simulation and experimentation are shown in Fig. 8.

2) Scheme 2: The MT-HVDC of Fig. 1 is considered for simulation and experimentation. GVD droop control is selected for the GS-VSCs while fixed ac voltage and active power control applied, to extract maximum power, at WF-VSCs. V_{dc-s} and V_{dc3-H} are set at 0.95pu and 1.05pu, respectively, and the droop characteristics are set as in scheme 1, that is, $k_3 = 10$ and k_4 is calculated as 4.29, 4.67 and 6.94 for transfer ratios of 2.33, 2.14 and 1.44, respectively.

Initially, wind power variation is observed, whence power from WF$_2$ rises to 0.4pu, power transfer through GS-VSC$_1$ and GS-VSC$_2$ change to -0.75pu and -0.35pu, respectively, via GVD control, to achieve equilibrium as shown in Fig. 9 for a transfer ratio 2.14. Consequently, the dc voltage settles at 1.02pu and P_{WF1} remains constant. The second half of Fig. 9 presents the case when the power demand from GS-VSC$_2$ changes to -0.45pu and in response P_{GS1} reduces to -0.65pu. The MT-HVDC system suffers from a power shortfall according to $m = 1.44$, thus the voltage level reduces to 1.01pu, while P_{WF1} and P_{WF2} remain unaffected.
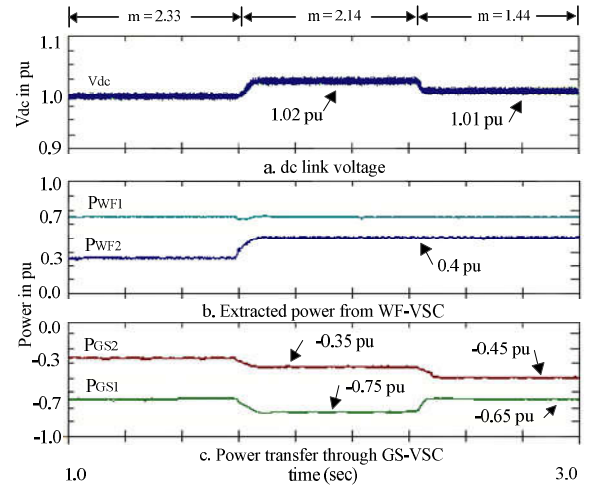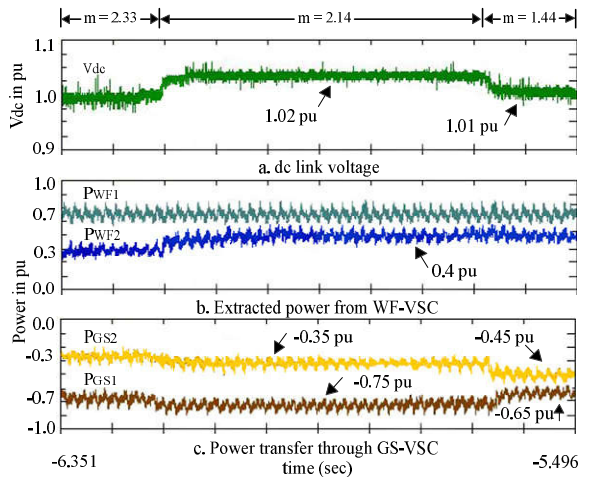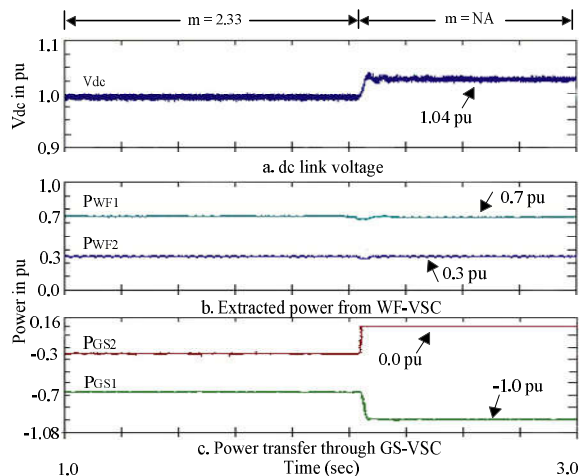

a.   Simulation results

b.   Experimental results

Fig. 9. DC link voltage and power during change in power from WF-VSC$_1$ and GSVSC$_1$ (test 1 and 2 - scheme 2).

For the third test, the proposed MT-HVDC undergoes disconnection of GS-VSC$_2$ as a permanent symmetrical fault

Table IV.
Comparison of injected and transmitted power for two schemes under three dynamic tests

	Scheme 1			Scheme 2		
	P_{WF} change	P_{GS} change	VSC disconn.	P_{WF} change	P_{GS} change	VSC disconn.
WF-VSC$_1$ (pu)	0.4	0.5	0.155	0.4	0.4	0.3
WF-VSC$_2$ (pu)	0.6	0.7	0.55	0.7	0.7	0.7
Total P_{WF} (pu)	1.0	1.2	0.7	1.1	1.1	1.0
GS-VSC$_1$ (pu)	-0.3	-0.5	0.0	-0.35	-0.45	0.0
GS-VSC$_2$ (pu)	-0.7	-0.7	-0.7	-0.75	-0.65	-1.0
Total P_{GS} (pu)	-1.0	-1.2	-0.7	1.1	1.1	-1.0
dc-link voltage	1.02 pu (1.0211)	0.99 pu (0.9986)	1.035 pu (1.0289)	1.02 pu (1.0150)	1.01 pu (1.0112)	1.04 pu (1.3990)
Power ratio (m)	1.5	1.44	3.66	2.14	1.44	NA

a.   Simulation results
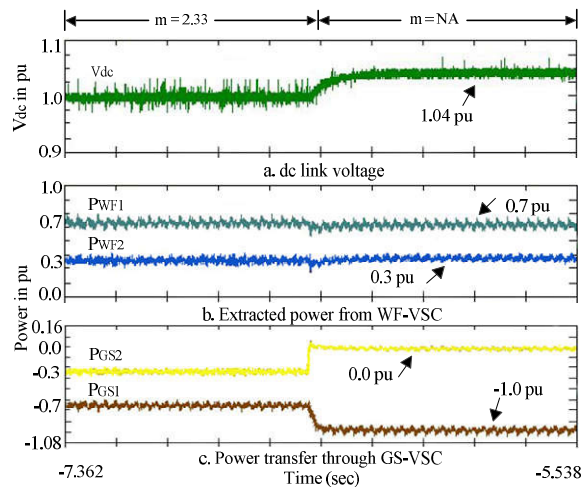
b.   Experimental results

Fig. 10. V_{dc} and P during change in power reference during disconnection of GS-VSC$_1$ to check the FRT capability of system (test 3 – scheme 2).

prevails on the connected ac network 1. Wind power extraction remains constant, causing system excess power. Power transfer through GS-VSC$_1$ increases to its maximum rating, that is -1.0 pu for $\varepsilon = 0.0015$ V, whilst maintaining V_{dc} within the permissible range of $\pm5\%$. This show the good FRT capability of the proposed strategy for MT-HVDC systems as in Fig. 10 while satisfying the FRT standards defined by Xu *et al.* [14].

The operation of the MT-HVDC for schemes 1 and 2 under all tests show that dc voltage control, power dispatch and FRT

capability of the designed control, is effective. Scheme 1 finds application when GS-VSCs are connected to weak ac grids and scheme 2 is applicable when maximum P_{WF} extraction is needed and the load center is distant. Table IV compares the injected power from the WF-VSCs into the MTDC grid and transmitted power of the GS-VSCs to the ac grids, and the dc-link voltages for the two schemes under the three controlled tests.

The values of analytical equations of section III are used to calculate the dc-link voltages, presented in brackets in Table IV. Calculated dc-link voltages match both simulated and experimental values, for both control schemes, under all three tests.

VI.   CONCLUSION

Flexible power dispatch and direct voltage control for VSC based multi-terminal HVDC systems have been proposed and analyzed in this paper. A generalized voltage droop control scheme was designed based on power transfer ratio to achieve flexible autonomous operation of VSC-HVDC stations. Two plausible control modes have been designed for a four terminal HVDC system. A new FRT strategy, based on active power sharing with GVD, is established, that does not require a special wind turbine design, extra hardware or telecommunication. EMTDC/PSCAD simulations and experimentation allowed assessment of grid control performance during wind power change, sudden load change, and permanent disconnection of a GS-VSC (because of a symmetrical ac grid fault), to verify the fault ride through capability of the MT-HVDC system for both control schemes. Simulation and experimental results demonstrate the merits of the power dispatch and direct voltage control during normal and abnormal conditions, satisfying the designed control schemes. Based on the simulations and experimental results, FRT capability of the MT-HVDC system is also enhanced.

REFERENCES

[1]   K. Rouzbehi, G. B. Gharehpetian, J. Candela, A. Luna, L. Harnefors, and P. Rodriguez, "Multi-terminal DC grids: operating analogies to ac power systems," *Renew. Sust. Ener. Rev.,* doi: 2016.11.270, Jul. 2016.
[2]   Lu, B. Ooi, "Premium quality power park based on multi-terminal HVDC", *IEEE Trans. Power Delivery*, vol. 2, pp. 978–983, 2005.
[3]   F. D. Bianchi and J. L. Domnguez-Garca, "Coordinated frequency control using mt-hvdc grids with wind power plants," *IEEE Trans. Sustain. Energy*, vol. 7, no. 1, pp. 213–220, Jan. 2016.

[4]   F. Longatt and J. Roldan, "Effects of dc voltage control strategy on voltage response on multi-terminal hvdc following loss of a converter station," 2013 IEEE PES General Meeting, Jul. 2013, pp. 1–5.

[5]   E. Prieto-Araujo, F. D. Bianchi, A. Junyent-Ferre, and O. GomisBellmunt, "Methodology for droop control dynamic analysis of multiterminal vsc-hvdc grids for offshore wind farms," *IEEE Trans. Power Del.*, vol. 26, no. 4, pp. 2476–2485, Oct. 2011.

[6]   K. Rouzbehi, A. Miranian, J. I. Candela, A. Luna, and P. Rodriguez, "A generalized voltage droop strategy for control of multiterminal dc grids," *IEEE Trans. Ind. Appl.,* vol. 51, no. 1, pp. 607–618, Jan. 2015.

[7]   T. M. Haileselassie and K. Uhlen, "Primary frequency control of remote grids connected by multi-terminal hvdc," IEEE PES General Meeting, Jul. 2010, pp. 1–6.

[8]   M. A. Abdelwahed and E. F. El-Saadany, "Power sharing control strategy of multi-terminal VSC-HVDC transmission systems utilizing adaptive voltage droop," *IEEE Trans. Sustain. Energy*, doi: TSTE.2016.2614223.

[9]   K. Rouzbehi, A. Miranian, A. Luna, and P. Rodriguez, "DC voltage control and power-sharing in multi-terminal DC grids based on optimal DC power flow and voltage droop strategy," *IEEE Journal of Emerging and Selected Topics in Power Electronics*, vol. 2, no. 4, pp. 1171–1180, Dec. 2014.

[10]   R. Eriksson, J. Beerten, M. Ghandhari, and R. Belmans, "Optimizing dc voltage droop settings for ac/dc system interactions," *IEEE Trans. Power Del.*, vol. 29, no. 1, pp. 362–369, Feb. 2014.

[11]   T. M. Haileselassie, "Control of Multi-terminal VSC-HVDC Systems", M.S. thesis, Dept. of Elec. Power Eng., Norwegian Univ. of Sci. and technol., Trondheim, Norway, 2008.

[12]   L. Xu, , L. Yao, M. Bazargan, B.W. Williams, "Control and operation of multi-terminal dc systems for integrating large offshore wind farms", *Proc. 7th int. Workshop on Large-Scale Integration of Wind Power and Transmission Networks for Offshore Wind Farms*, Spain, May 2008.

[13]   L. Xu, L. Yao, M. Bazargan, "DC grid management of a multi-terminal hvdc transmission system for large offshore wind farms", *Proc. First SUPERGEN Conf.*, Nanjing, China, April 2009.

[14]   L. Xu and L. Yao, "DC voltage control and power dispatch of a multiterminal HVDC system for integrating large offshore wind farms," *IET Renew. Power Gen.*, vol. 5, no. 3, pp. 223–233, 2011.

[15]   A. Egea-Alvarez, F. Bianchi, A. Junyent-Ferre, G. Gross, O. Gomis-Bellmunt, "Voltage control of multi-terminal VSC-HVDC transmission systems for offshore wind power plants: design and implementation in a Scaled Platform, " *IEEE Trans. Ind. Electron.*, vol. 60, no. 6, pp.2381-2391, Jun. 2013.

[16]   A. Raza, X. Dianguo, L. Yuchao, S. Xunwen, B. W. Williams and C. Cecati, "Coordinated Operation and Control of VSC Based Multiterminal High Voltage DC Transmission Systems," *IEEE Trans. on Sustain. Energy*, vol. 7, no. 1, pp. 364–373, Jan. 2016.

[17]   J. Liang, T. Jing, O. G. Bellmunt, J. Ekanayake, and N. Jenkins, "Operation and control of multiterminal HVDC transmission for offshore wind farms," *IEEE Trans. Power Del.*, vol. 26, pp. 2596-2604, Oct. 2011.

[18]   K. Rouzbehi, A. Miranian, J.I. Candela, A. Luna, P. Rodriguez, "A Generalized Voltage Droop Strategy for Control of Multiterminal DC Grids," *IEEE Trans. Ind. Appl.*, vol.51, no.1, pp. 607–618, Jan./Feb. 2015.

[19]   L. Xu, L. Yao, C Sasse, "Grid integration of large DFIG based wind farms using VSC transmission", *IEEE Trans. Power Syst.*, vol. 22, no. 3, pp. 976–984, 2007.

[20]   G. Ramtharan, A. Arulampalam, J. Ekanayake, F. Hughes, N. Jenkins, "Fault ride through of fully rated converter wind turbines with AC and DC transmission systems", *IET Renew. Power Gener.*, vol. 3, pp. 426–428, 2009.

[21]   L. Harnefors, Y. Jiang-Ha¨fner, M. Hyttinen, T. Jonsson, "Ride through methods for wind farms connected to the grid via a VSC HVDC transmission," *Proc. 2007 Nordic Wind Power Conf.*, pp. 1–5.

[22]   L. Xu, B. Andersen, "Grid connection of large offshore wind farms using HVDC", *Wind Energy*, vol. 9, no. 4, pp. 371–382, 2006.